INTERNATIONAL JOURNAL FOR NUMERICAL AND ANALYTICAL METHODS IN GEOMECHANICS
Int. J. Numer. Anal. Meth. Geomech., 2000; **24**:533–565

Extrusion movements of a tunnel head reinforced by finite length bolts—a closed-form solution using homogenization approach

Henry Wong[1], Didier Subrin[1] and Daniel Dias[2]

[1] *Laboratoire Géomatériaux, Département Génie Civil et Bâtiment, Ecole Nationale des Travaux Publics de l'Etat, rue Maurice Audin, 69518 Vaulx-en-Velin Cedex, France (CNRS URA 1652)*
[2] *URGC Géotechnique, Institut National des Sciences Appliquées de Lyon, avenue Albert Einstein, 69621 Villeurbanne, France*

SUMMARY

An analytical model on the general behaviour of a tunnel head, reinforced by finite length bolts is proposed. This model is based on the homogenization method and spherical symmetry assumption. Despite its simplicity, and in consequence its limits of validity, it does allow a quick estimation of the key design parameters: frontal displacement, extension of decompressed zone, ground stresses and bolt tension, and constitutes thereby a very useful and handy tool for design engineers. In particular, the influence of the reinforcement length, as well as other important design parameters, are studied by the proposed model. The charts resulting from the parametric studies are directly applicable. Otherwise, the comparison to a 3D numerical model is also presented in this paper. The first results provide the validation of the analytical solution, at least in terms of average extrusion movements. Copyright © 2000 John Wiley & Sons, Ltd.

KEY WORDS: bolts; tunnels; composite; homogenization; analytical solution; elastoplasticity

1. INTRODUCTION

The problem of tunnel head instability, and its proper prevention by an adequate reinforcement, is an important subject in the area of underground works, due to the dramatic consequences of a frontal failure: loss of human lives and equipment, execution delays, ruin of surface structures, etc. Beyond the question of stability, it is equally important to limit the ground movements ahead of the front, as any volume loss can generate surface settlements and in consequence lead to damages of surface structures or nearby underground works within the zone of influence. In the case of sensitive materials, excessive displacements—hence strains—can also undermine significantly the material strength, thereby reducing the stability, and eventually trigger off an early failure, precisely due to the strength reduction.

*Correspondence to: H. Wong, Laboratoire Géomatériaux, Département Génie Civil et Bâtiment, Ecole Nationale des Travaux Publics de l'Etat, rue Maurice Audin, 69518 Vaulx-en-Velin Cedex, France (CNRS URA 1652)

Contract/grant sponsor: French National Tunneling Research Center (Centre d'Etudes des Tunnels, CETU).

Received 21 August 1997
Revised 30 August 1999

Table I. Examples of tunnel projects using fibre-glass bolts for face reinforcement

Year	State	Project	Length (m)
1988	Italy	HST Link Roma–Fiorenze (5 tunnels[3])	7370
1989	Italy	Targia–Siracusa (Tunnel di Siracusa)	1000
1990–91	France	HST Link (Tunnel de La Galaure)	
1991	Italy	Caserta–Foggia (Tunnel San Vitale[4])	1300
1993	Italy	Ancona–Bari (Tunnel Vasto)	4970
1995	Greece	Metro Athens (a few tunnels)†	
1995–97	Portugal	Metro Lisboa†	
1996–97	Lebanon	Hydraulic Tunnel of Haret†	
1996–97	Colombia	Carretera Bogota (Road Tunnel)†	
1997–98	France	HST Link Lyon–Marseille (Tunnel de Tartaiguille[5,31])	2330
under progress	France	Cross-town Tunnel of Toulon	1200×2
under progress	Italy	HST Link Bologna–Fiorenze	

† Private communication from SIREG s.p.a. Milano, Italy (fibre-glass bolts manufacturer)

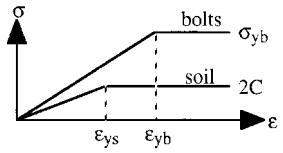

Figure 1. Conceptual representation of soil and bolt behaviours.

From the construction standpoint, different techniques of pre-lining or reinforcement of tunnel heads have been proposed,[1] amongst which use of fully grouted fibre-glass bolts presents a few advantages,[2] notably their high longitudinal ultimate strength and the facility of removal during excavation, as well as the facility to adapt locally the reinforcement density to local geotechnical conditions. Such advantages have indeed contributed to the increasing popularity among geotechnical engineers of this fastly emerging technique, especially in France and Italy, as witnessed by its increasing use in tunneling projects[3–5] (Table I). On the other hand, their relatively large flexibility results in a slow and progressive force build-up, in such a way that their strength capacity can be fully mobilized only at relatively large strains (Figure 1). Their effective contribution depends therefore much on the ductility of *in situ* material and loading conditions. Design methods, using either a hypothetical fictive frontal pressure, or an isotropic increase of strength—both of them calculated by supposing the bolts working at their limit load[6]—can thus be dangerously optimistic. Moreover, taking into account the construction phases (installation of bolts, excavation, shotcrating), the length of the bolts varies with the advancement of works. *It is therefore important to ensure that the designed bolt length is adequate at all phases of work, and at the same time sufficiently optimized for economic reasons.*

In regard to modelling and design aspects, a small number of analytical models exist, which analyse the tunnel head stability, in the case of isotropic and homogeneous materials. The majority of such models are based on limit analysis and yield design theory,[7] leading to lower or upper bound estimates on the safety margin.[8,9] In order to simplify the three-dimensional problem, some authors assimilate the excavation front to a spherical cavity (Figure 2 without

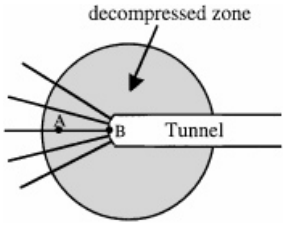

Figure 2. Schematic representation of the problem geometry.

bolt), to make the problem amenable to analytical treatments.[10] Based on rigid-plastic behaviour, these models do not, however, allow any quantitative deduction on the movement of extrusion of the tunnel head—an important design parameter by itself—nor on the contribution of bolts.

Concerning the proper modelling of the composite: soil + reinforcement, 3D numerical approches have been proposed: the majority of them model each bolt individually.[11] Over such 'heterogeneous' approaches, the homogenization method[12,13] presents interesting possibilities, and has been applied to the lining analysis of tunnels[14,15] within the framework of the Convergence-Confinement method.[16,17]

However, as the foregoing discussions well indicated, analytical treatment of the behaviour of a bolted tunnel head, within the framework of these models, must take into account the following important considerations: firstly, the non-simultaneous yielding of the medium and the bolts has an important bearing on the displacements. Secondly, the evolutive character of the tunnel head is difficult to model, not to mention the fundamentally different geometry—spherical instead of cylindrical, giving rise to corner-flow plastic zones.

To overcome such difficulties, we will suppose firstly that the stress path followed by a point such as A (Figure 2), initially far ahead of the front and outcrops at a later instant as excavation proceeds, is the same as the stress path followed by a point B on stationary front, while a monotone decreasing pressure (varying from the initial overburden to zero) is applied. Secondly, the bolts are supposed to be disposed in a radial direction, perpendicular to the spherical front of radius R, and perfectly bonded to the surrounding soil mass. This allows the assumption of spherical symmetry of all mechanical quantities ahead of the front to be consistently made. Finally, the homogenization process undertaken does account for the delayed plastification of the bolts, leading to a strain hardening macroscopic behaviour.

Note that the spherical assumption basically applies to the near field, where variations of field quantities are significant. Outside a certain characteristic length L_{crit}, the precision of this assumption gets worse, when they do not have any more significant influence on the near-field behaviour (extrusion movement and stress changes). In the same spirit, the radially disposed bolts introduce an artificial decreasing reinforcement density (Figure 2) which does not exist in reality (Figure 20). Nonetheless, the most important changes take place at the near field, where the bolt density variation is limited. The concordance with other more sophisticated numerical methods provides an *a posteriori* justification to this assumption. It should also be mentioned that the spherical symmetry assumption does not limit the model to circular tunnels; other shapes 'not too far' from circular (square, horse-shoe, elliptical, etc.) can reasonably be considered as acceptable, in similar spirits to the convergence-confinement method.[16,17]

The homogenization method, together with the perfect bonding assumption (soil–bolt interface), basically amounts to say that the displacement field is 'smooth', local fluctuations due to stiffness contrasts being negligible. This assumption is valid when the bolt density is 'high', or more precisely when the characteristic distance between neighbouring bolts (noted l) is much less than the characteristic dimension of the problem (the tunnel diameter D in the present case). In theory, $D/l > 10$ is a 'safe' limit, while in practice, values of D/l from 4 to 5 are considered acceptable.[18] In practice, this means that local instabilities or deformation modes cannot be treated by the proposed model; only the global displacement-reduction effects are analysed.

On the other hand, in order to investigate the influence of bolt lengths—a parameter of important economical bearings as well as mechanical implications—*the present model takes into account finite bolt-lengths*, contrary to previous publications.[19–21]

While the different hypotheses limit the domain of validity of the model, they allow, on the other hand, explicit solutions to be found which present great advantages over more sophisticated approaches. The present analytical model should, for example, be compared to the solution proposed by Jassionnesse *et al.*,[22,23] where the causality link between input parameters and the structural response is less transparent due to the semi-numerical character.

Furthermore, the present theoretical solution has been compared to a 3D numerical model, developed by Dias.[11] The results of the comparison, presented in the last part of this article, provide the verification of the analytical model and allow to delimit the domain of validity of the theory.

2. IDEALIZED PROBLEM

On account of the previous hypotheses, the idealized problem to be solved is the following. In an infinite, homogeneous but anisotropic medium (due to bolts), with zero initial displacements and strains, but a non-zero homogeneous and isotropic stress field $\boldsymbol{\sigma}_\infty = -P_\infty \mathbf{1}$, is created a spherical cavity. On the wall of this cavity is applied a variable internal pressure P_i, which decreases monotonically from P_∞ to 0, and we are interested in the evolution of the various physical quantities (displacements, stresses, and development of plasticity within each of the constituents), in particular when P_i comes to zero—in other words, when point A of Figure 2 outcrops at the front.

Note that the framework of main assumptions adopted (excepted homogenization) follow closely that of the convergence-confinement method.[16,17] In particular, the hypotheses of homogeneity and isotropy of the initial stress field only apply for deep tunnels in isotropic ground, with a coefficient of at rest earth pressure K_0 close to unity. Any significant deviation from such hypotheses will, of course, lead to computational inaccuracies. Nonetheless, just as the convergence-confinement method, when applied with caution and properly interpreted, the model remains a very useful tool for quick preliminary designs.

3. THE CONSTITUTIVE EQUATIONS

The bolts are supposed to be elastic–perfectly plastic and in a pure tensile state, with zero stiffness and strength with respect to moment and shear. Their mechanical behaviour can thus be described by four parameters E_b, σ_{yb}, S_b and d_b, respectively Young's modulus, uniaxial tensile

strength, cross-sectional area and density (number of bolts per m^2 at the excavation front), $T_{yb} = \sigma_{yb} S_b$ being the ultimate tensile strength of one bolt.

The ground, equally elastic–perfectly plastic, is supposed to obey the Tresca's criterion and its associated flow rule. It is therefore characterized by three parameters: C, E_s and ν_s (or equivalently μ_s and λ_s—the Lamé constants), C being the soil cohesion while E_s and ν_s are Young's modulus and Poisson's ratio of the ground. Basically, this limits the present model to the case of short-term behaviour of clayey or marly formations where the frictional component is not significant, in other words, internal friction angle is near zero. This restriction has, however, been removed by the development of another model based on Mohr–Coulomb criterion, taking into account a non-zero dilation. This second model is, nonetheless, more complex, and is still being tested at the time of writing the present paper. The bolts are supposed to be perfectly bonded to the surrounding ground, and follow the same displacement field. Their tensile stress therefore only depends on the longitudinal strain in the direction parallel to the bolt axis.

Under such conditions, the stress tensor of the equivalent homogeneous material can be considered as the sum of two components,[12] due, respectively, to soil and bolts:

$$\boldsymbol{\sigma} = \boldsymbol{\sigma}_s + \boldsymbol{\sigma}_b$$

3.1. Elastic behaviour

Under elastic behaviour, the stresses induced in the ground by the strain field $\boldsymbol{\epsilon}$ writes

$$\boldsymbol{\sigma}_s = 2\mu_s \boldsymbol{\epsilon} + \lambda_s \operatorname{tr}(\boldsymbol{\epsilon})\mathbf{1} - P_\infty \mathbf{1}$$

where $-P_\infty \mathbf{1}$ is the initial isotropic stress due to overburden. Subjected to the same strain field $\boldsymbol{\epsilon}$, and on account of the particular disposition of the bolts, the bolt stress is given by $\sigma_b = E_b \varepsilon_{rr} \leqslant \sigma_{yb}$ (to be distinguished from the homogenized stress tensor $\boldsymbol{\sigma}_b$), and the tensile force $T_b = S_b E_b \varepsilon_{rr} \leqslant T_{yb} = S_b \sigma_{yb}$. At a distance r from the centre, the tributary area per bolt is given by $A = (r^2/R^2)/d_b$, hence the homogenized radial stress is given by $\sigma_0(r) = T_b/A = d_b S_b E_b \varepsilon_{rr} (R/r)^2 \leqslant d_b S_b \sigma_{yb} (R/r)^2$. The homogenized uniaxial stress tensor due to bolts therefore writes

$$\boldsymbol{\sigma}_b = d_b S_b E_b \varepsilon_{rr} \left(\frac{R}{r}\right)^2 \mathbf{e}_r \otimes \mathbf{e}_r \quad \text{for elastic behaviour}$$

$$\boldsymbol{\sigma}_b = d_b S_b \sigma_{yb} \left(\frac{R}{r}\right)^2 \mathbf{e}_r \otimes \mathbf{e}_r \quad \text{if bolt has yielded at the radius } r$$

in spherical co-ordinates (r, θ, ϕ) where R is the radius of the spherical front, ε_{rr} the radial strain and $\mathbf{e}_r$ the unit radial vector. Spherical symmetry, together with the incompressibility assumption of the ground ($\nu_s = 0{\cdot}5$), allow to simplify the equation relating the non-zero macroscopic stress rates to the strain rates to the following:[19,20]

$$\begin{bmatrix} \dot{\varepsilon}_{rr} \\ \dot{\varepsilon}_{\theta\theta} \end{bmatrix} = \left\{ E_s \left(1 + \frac{k^2}{r^2}\right) \right\}^{-1} \begin{bmatrix} 1 & -1 \\ -1/2 & 1/2 \end{bmatrix} \begin{bmatrix} \dot{\sigma}_{rr} \\ \dot{\sigma}_{\theta\theta} \end{bmatrix} \tag{1}$$

where $k^2 = (d_b S_b (E_b/E_s))R^2 = \beta R^2$. Here, the parameter β which can also be written in the form $\Delta E/E_s$, is an essential dimensionless parameter which characterizes the stiffness contribution from the bolts. To simplify notations, we will simply write σ_r instead of σ_{rr}, etc.

3.2. Plastic behaviour

To describe the plastic behaviour, two information are needed: the yield criterion and the plastic potential. On account of the spherical symmetry, the loading mode $\dot{P}_i < 0$ (i.e. the internal pressure is monotone decreasing, so that the radial stress is the major principal stress), and the corner flow condition $\sigma_\theta = \sigma_\phi$, the yield criterion in the absence of reinforcement can be written as

$$f(\boldsymbol{\sigma}) = \sigma_r - \sigma_\theta - 2C \tag{2}$$

where by convention $f < 0$ represents the elastic domain. When bolts are present, they tend to take up part of the radial tensile stresses, thereby reducing the part which has to be taken up by the ground. Hence, from the macroscopic behaviour standpoint, an additional term $\sigma_0(r)$, representing the strength contribution due to bolt tensions, has to be added to (2). Since $\sigma_0(r)$, the homogenized tensile stress taken up by the bolts, depends on the radial strain, and yielding of bolts and ground occurs non-simultaneously, we therefore have to distinguish two qualitatively different plastic zones: PL1 (ground yielded but not the bolts) and PL2 (both yielded) in which $\sigma_0(r)$ takes different forms:

$$\text{PL1,}\quad \varepsilon_r < \varepsilon_{yb} : \sigma_0(r) = \frac{k^2}{r^2} E_s \varepsilon_r \rightarrow f(\boldsymbol{\sigma}) = \sigma_r - \sigma_\theta - 2C - \frac{k^2}{r^2} E_s \varepsilon_r \tag{3}$$

$$\text{PL2,}\quad \varepsilon_r > \varepsilon_{yb} : \sigma_0(r) = \frac{k^2}{r^2} \frac{E_s}{E_b} \sigma_{yb} \rightarrow f(\boldsymbol{\sigma}) = \sigma_r - \sigma_\theta - 2C - \frac{k^2}{r^2} \frac{E_s}{E_b} \sigma_{yb} \tag{4}$$

where σ_{yb} is the yield stress and $\varepsilon_{yb} = \sigma_{yb}/E_b$ the yield strain of the bolts. On the other hand, the associative plastic potential and the corner flow condition lead to

$$\dot{\boldsymbol{\epsilon}}^p = \frac{1}{2} \dot{\zeta} (\partial_{\boldsymbol{\sigma}} f_{r\theta} + \partial_{\boldsymbol{\sigma}} f_{r\phi}) = \dot{\zeta} \begin{bmatrix} 1 & 0 & 0 \\ 0 & -\frac{1}{2} & 0 \\ 0 & 0 & -\frac{1}{2} \end{bmatrix} \tag{5}$$

4. FUNDAMENTAL EQUATIONS

On account of the compatibility equations $\varepsilon_r = \partial_r u$ and $\varepsilon_\theta = u/r$, and of the form of $\dot{\boldsymbol{\epsilon}}^e$ and $\dot{\boldsymbol{\epsilon}}^p$ (equations (1) and (5)), an integration of the relation $\dot{\boldsymbol{\epsilon}} = \dot{\boldsymbol{\epsilon}}^e + \dot{\boldsymbol{\epsilon}}^p$ between the initial reference state, at which displacements and strains are zero while the *in situ* stress is $-P_\infty \mathbf{1}$, and the current state, leads to the following constitutive equations of our problem:

$$\partial_r u = \left[E_s \left(1 + \frac{k^2}{r^2} \right) \right]^{-1} (\sigma_r - \sigma_\theta) + \zeta \tag{6}$$

$$\frac{u}{r} = \left[2E_s \left(1 + \frac{k^2}{r^2} \right) \right]^{-1} (\sigma_\theta - \sigma_r) - \frac{\zeta}{2} \tag{7}$$

to which must be added the equilibrium equation:

$$r\partial_r\sigma_r + 2(\sigma_r - \sigma_\theta) = 0 \tag{8}$$

and one of the three forms (2), (3) or (4) for the yield criterion.

The loading condition coincides here with the boundary condition at the front:

$$\sigma_r(R) = -P_i \tag{9}$$

with P_i varying monotonically from P_∞ to zero. However, it turns out to be simpler to work with a positive loading parameter ΔP defined by

$$\Delta P = P_\infty - P_i, \quad \Delta P^* = \frac{\Delta P}{C} \tag{10}$$

The six equations (2)–(8) are the fundamental equations of our problem. A variable-count shows that the number of equations is always equal to the number of unknown variables, and the problem is therefore well defined. For example, in an elastic zone, there are three unknowns (u, σ_r, σ_θ with $\zeta = 0$) and the three equations (6)–(8) apply. In a plastic zone, we have an additional unknown since $\zeta \neq 0$, but also an additional equation (either (2), (3) or (4)).

It should be noted that on account of the incompressibility assumption and the Tresca flow rule, the volumetric strain is identically zero, and the displacement field always satisfies $\partial_r u + 2u/r = 0$, independently of material behaviour, leading to

$$u = -\frac{B}{r^2}; \quad \varepsilon_r = \partial_r u = \frac{2B}{r^3} \tag{11}$$

(B = constant of integration related implicitly to the loading parameter ΔP) which simplifies greatly the solution process.

5. SCENARIOS

For comprehension purpose, as well as for latter reference, it would be helpful to describe at present the sequence of events, notably the evolution of the plastic zones, without proof. When the internal pressure decreases (thus $\Delta P = P_\infty - P_i$ increases), the medium remains entirely elastic for a while, until the yield criterion of the ground is reached at $x = R$, when $\Delta P = \Delta P^{(1)}$. A first plastic zone PL1, in which yielding of the medium has occurred while the bolts remain elastic, then appears at the front and develops. When ΔP reaches a second critical value $\Delta P^{(2)}$, the bolts also yield at the front, and a second plastic zone PL2 evolves from the front and develops. At a third critical value $\Delta P^{(3)}$, the plastic zone PL1 reaches the limit of the reinforced zone, such that an instant later four different zones co-exist (PL2, PL1, PL3, EL) where PL3 corresponds to the newly appeared, unreinforced plastic zone. Finally, the last phase intervenes when the fourth critical value $\Delta P^{(4)}$ is reached and yielding of the bolts occurs over their entire length (i.e. the plastic radius z reaches R_b). This sequence of events: configurations 1–5, is illustrated in Figure 3. Note that such kind of evolution of elastoplastic zones is common, and has already been encountered elsewhere.[15,24,25]

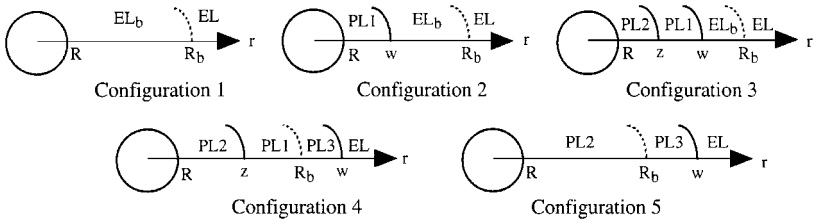

Figure 3. Evolution of plastic zones (Case A, long bolts). $R_b = R + L_b$.

The above illustration is valid for very long bolts (large values of L_b). Depending on this last parameter, two different evolutions are in fact possible. Either yielding of the bolts at $r = R$ takes place first, before the front of PL1, w, reaches the limit of the reinforced zone defined by $R_b = R + L_b$ (case A described above), or the reverse occurs (case B). These two cases are graphically shown in Figure 4 below, which is a complementary representation to Figure 3.

6. RESOLUTION FOR EACH CONFIGURATION

The problem has to be solved for each of the six different configurations encountered (Figure 4). For a particular configuration, a set of differential equations apply to each zone. Elimination allows to single out the two main unknowns: the displacement u and the radial stress σ_r, which satisfy two differential equations. The assumption $v_s = 0{\cdot}5$ uncouples the system in all cases, and leads to a single differential equation on σ_r, which hopefully admits an explicit solution (otherwise, no global analytical solution can be found) comprising unknown constants of integration. These unknown constants can be solved in each zone using the appropriate boundary conditions—yielding of soil or bolts, or condition at infinity. The unknown plastic boundaries are finally determined by imposing the continuity of σ_r at these points. The other quantities are then determined by simple substitution.

For clarity of presentation, the detailed solution process is reported to Appendix I, and the detailed expressions (displacement, stresses, strains) in each zone and in each configuration are grouped together in corresponding tables there.

Tables II–V summarize the key results obtained.

The simplicity of the analytical solution so obtained is remarkable, and deserves a few comments:

(1) When $b \to \infty$, we get the same results as Wong *et al.*,[19–21] demonstrating the consistency of the present solution with the limiting case of infinite bolt lengths.
(2) For both cases A and B, the transition between successive configurations have been shown to be consistent, and all respect the transition case of $b^3 = \varepsilon^*$.
(3) While the radial stress is continuous, as is required by local equilibrium, tangential stress σ_θ and plastic strain ζ are, on the other hand, discontinuous across the radius R_b (so is the elastic radial strain, as the total strain $\varepsilon_r = 2B/r^3$ is continuous). Such discontinuities are expected as perfect bonding between bolts and ground implies a jump of stiffness as well as strength across R_b.

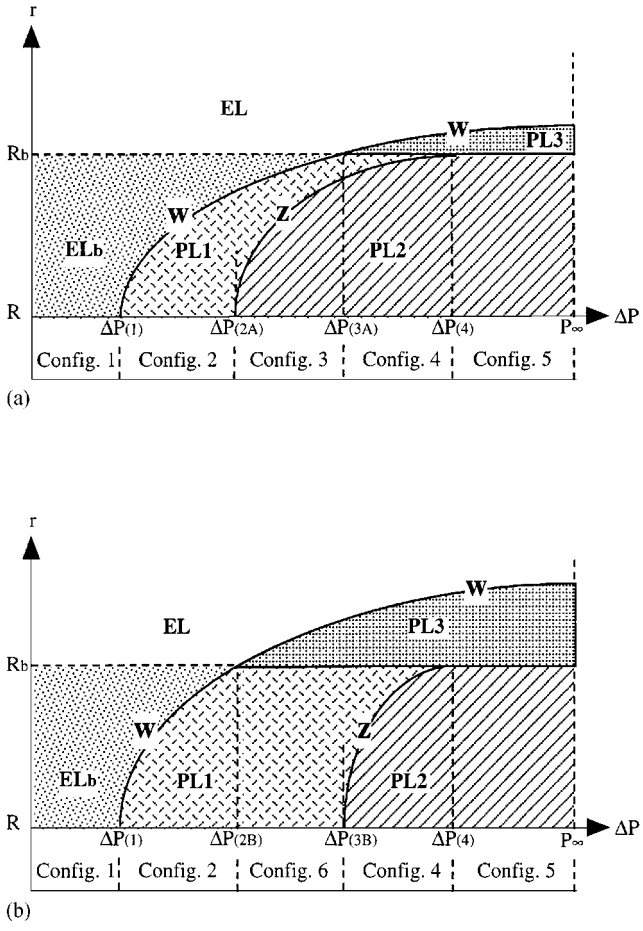

Figure 4(a). Evolution of plastic zones in case A—bolts yielded at R before plastic zones PL1 reaches R_b. (b) Evolution of plastic zones in case B—plastic zone PL1 reaches R_b before bolts yielded at R.

Table II. Transition values of the dimensionless loading parameter ΔP^* for cases A and B

Case A ($b^3 > \varepsilon^*$)	Case B ($b^3 < \varepsilon^*$)
$\Delta P^{*(1)} = \frac{4}{3}\{1 + \frac{3}{5}\beta[1 - b^{-5}]\}$	
$\Delta P^{*(2A)} = \frac{4}{3} + \frac{4}{3}\,\mathrm{Ln}(\varepsilon^*) + \frac{4}{5}\beta[1 - b^{-5}]\,\varepsilon^*$	$\Delta P^{*(2B)} = \frac{4}{3} + \frac{4}{3}\,\mathrm{Ln}(b^3) + \frac{4}{5}\beta[1 - b^{-5}]\,b^3$
$\Delta P^{*(3A)} = \frac{4}{3} + \frac{4}{3}\,\mathrm{Ln}(b^3) + \Omega\left[1 - \frac{3}{5}\frac{\varepsilon^{*2/3}}{b^2}\right] - \frac{4}{5}\beta\,b^{-2}$	$\Delta P^{*(3B)}$ same expression as $\Delta P^{*(2A)}$
$\Delta P^{*(4)} = \frac{4}{3}\,[1 + \mathrm{Ln}(\varepsilon^* b^3)] + \Omega(1 - b^{-2})$	

Table III. Equations determining the unknown plastic boundaries

Configuration	Equations determining the unknown plastic boundaries
2	$\Delta P^* = \frac{4}{3} + 4\,\mathrm{Ln}\,W + \frac{4}{5}\beta[1 - b^{-5}]W^3$
3	$\Delta P^* = \frac{4}{3} + 4\,\mathrm{Ln}\,W + \Omega\left[1 - \frac{3}{5}\frac{\varepsilon^{*2/3}}{W^2}\right] - \frac{4}{5}\beta b^{-5}W^3;\ Z = \frac{W}{\varepsilon^{*1/3}}$
4	same equations as in Configuration 3
5	$\Delta P^* = \frac{4}{3} + 4\,\mathrm{Ln}\,W + \Omega[1 - b^{-2}] \Leftrightarrow W = \mathrm{Exp}\left[\frac{\Delta P^*}{4} - \left\{\frac{1}{3} + \frac{\Omega}{4}(1 - b^{-2})\right\}\right]$
6	same equation as in Configuration 2

Table IV. Displacement $u(R)$ at the excavation front in different configurations

Configuration	Displacement at the front $u(R)$
1	$\frac{E_s}{C}\frac{u(R)}{R} = -\Delta P^*\left[\frac{4}{5}\beta[1 - b^{-5}] + \frac{4}{3}\right]^{-1}$
All others	$\frac{E_s}{C}\frac{u(R)}{R} = -W^3$; W being the solution of equations in Table II

Table V. Tension in bolts. $W = w/R$ is the boundary of the decompressed zone (soil yielded), given by the solution of equations in Table II

Configuration	zone	Bolt tension $T_b^* = \frac{d_b}{C}T_b$
1	EL_b	$2\beta\frac{\Delta P^*}{\Delta P^{*(1)}}\left(\frac{R^3}{r^3}\right)$
2 à 6	PL1 or EL_b	$2\ \beta\ W^3\left(\frac{R^3}{r^3}\right)$
2 à 6	PL2	Ω

(4) Perfect bonding between ground and bolts implies that the bolt axial strain and stress is decreasing with r, hence bolt tensions are maximum at the front. This is in fact only a gross approximation. In reality, for finite bond strengths, the tension should be zero at the front and climb to a maximum at some distance ahead of the front, before decreasing progressively to zero. For sufficiently high bond strengths, this approximation is acceptable, while for low bond strengths, the results require careful interpretations.

(5) It is remarkable that the evolution of the exterior plastic radius w, and by consequence also the extrusion displacement, is governed by the same equation in Configurations 3 and 4 (respectively in Configurations 2 and 6). In other words, there is no discontinuity in the displacement and strain behavior when the yielded (decompressed) zone sweeps across the

radius R_b so that yielding occurs in the outer (unreinforced) zone. This means, at least according to this model, that the reinforced zone acts as a lining which opposes to extrusion movements, rather than relying on the bolt tensions developed by the anchorage into the medium ahead of the front. This may appear to be a disagreement with ordinary intuitive practice, which tends to design bolt lengths so that they go beyond the yielded (decompressed) zone. This observation should however be further examined, taking into account finite bond strengths, and their possible degradation with ground decompression.

(6) Under spherical symmetry, the convergence $u(R)$ is of course identical at every point on the surface, which is not the case for the tunnel head. The displacement so calculated should therefore be compared to the 'average' frontal displacement (ground loss divided by the tunnel head surface). It should also be borne in mind that the lining behind the front has a non-negligible influence on the frontal displacements, while this effect is simply impossible to account for under spherical symmetry. The numerical results must therefore be interpreted with caution.

Although the hypotheses involved do put limits on the precision of the model (last remark), the latter remains nonetheless a very precious tool for sensitivity analyses and preliminary design, as the following sections will demonstrate.

7. PARAMETRIC STUDY

A relatively restricted parameter study will be presented, which should highlight the influence of the 'reinforcement parameters' (i.e. β, Ω and b), on the structural response. Since we are interested by the maximum extrusion movement, which occurs at the end of the stress history when $P_i = 0$, or in other words when $\Delta P^* = P_\infty/C = P^*$, this last value should be substituted at the place of ΔP^* in the various formulae.

7.1. Essential dimensionless parameters

We have seen that the plastic radii $W = w/R$ and $Z = z/R$ are implicitly defined by equations of the form $P^* = H(W, \beta, \Omega, b)$, hence we can write $W = F(P^*, \beta, \Omega, b)$, and similarly for $Z = z/R$, while the front displacement writes $U^* = (E_s/C)(u(R)/R) = G(P^*, \beta, \Omega, b)$, where the latter becomes $P^* g(\beta, \Omega, b)$ under elastic behaviour (i.e. linearity between u and P^*). The bolt tension, in its dimensionless form $T_b^* = T_b(d_b/C)$, is given by the formulae in Table IV. The structural response therefore depends on four essential dimensionless parameters: P^*, β, Ω, and b. Recall that P^* represents the effect of geostatic pressure, while β and Ω are the contributions of bolts in terms of stiffness and strength, and b the effect of bolt length.

7.2. Range of 'realistic' dimensionless parameters

To avoid treating unrealistic values, the parametric studies in the following paragraphs will be limited to a reasonable range of 'typical' parameters. For the ground, the range of variation will be taken to be $60\ \text{MPa} < E_s < 3000\ \text{MPa}$, $0{\cdot}15\ \text{MPa} < C < 2{\cdot}5\ \text{MPa}$, while we will consider typical fibre-glass bolts, with: $S_b \approx 1500\ \text{mm}^2$; $E_b \approx 20000\ \text{MPa}$; $\sigma_{yb} \approx 500\ \text{MPa}$ with a fairly high bolt-density $d_b \approx 1\ \text{bolt/m}^2$. The reinforcement parameters will therefore be limited to

$$0{\cdot}01 < \beta < 0{\cdot}5, \qquad 0{\cdot}3 < \Omega < 5$$

For the ratio $P^* = P_\infty/C$, which is actually the inverse of the 'stability factor'—commonly defined as the ratio overburden vs. material strength, values above 5 can be considered as exceptional. We will therefore limit ourselves to values $P^* < 7$.

7.3. Bolt contribution under elastic behaviour

We will first show how the bolts delay yielding of ground, and the effects of bolt length.

Figure 5 shows the variation of $\Delta P^{*(1)}$ vs. the dimensionless bolt length L_b/R, for five different values of β (recall that $\Delta P^{*(1)} = \frac{4}{3} + \frac{4}{5}\beta\ [1 - b^{-5}]$ where $b = (R + L_b)/R = 1 + R_b/R$). It can readily be seen that, whatever is the value of β, any increase of bolt length beyond a radius is inefficient. For mediocre ground properties reinforced by fibre glass inclusion, for example with $E_s = 100$ MPa, $d_b = 1$ bolt/m^2, $S_b = 1500$ mm^2, $E_b = 20000$ MPa, giving $\beta = 0{\cdot}3$, the effect on the yield load is marginal (increase of $\Delta P^{*(1)}$ less than 20 per cent).

Similarly, the normalized extrusion movement in the elastic range is given by

$$\frac{E_s}{4\Delta P}\frac{u(R)}{R} = \left[\frac{\beta}{5}(1 - b^{-5}) + \frac{1}{3}\right]^{-1}$$

and is shown graphically in Figure 6.

The same remarks as above apply. For $\beta = 0{\cdot}3$, the relative reduction of displacement is limited to 15 per cent. As we will see below, the contribution of bolts is above-all significant under plastic behaviour.

7.4. Bolt contribution under general elastoplastic behaviour

In the following paragraphs, a parametric study will be carried out on the three key design parameters:

(1) the extension of the decompressed zone $W = w/R$ (i.e. plastic zone in which soil has yielded),

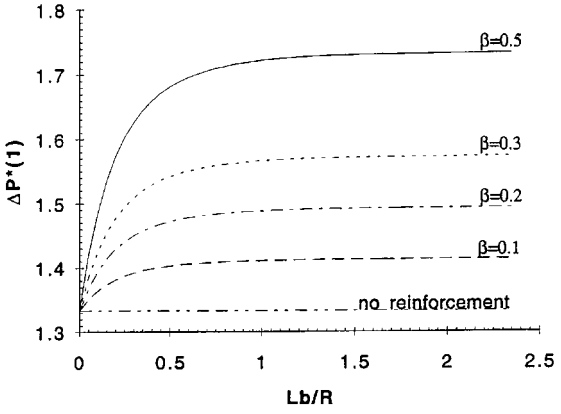

Figure 5. Influence of stiffness and length of bolts on yield load.

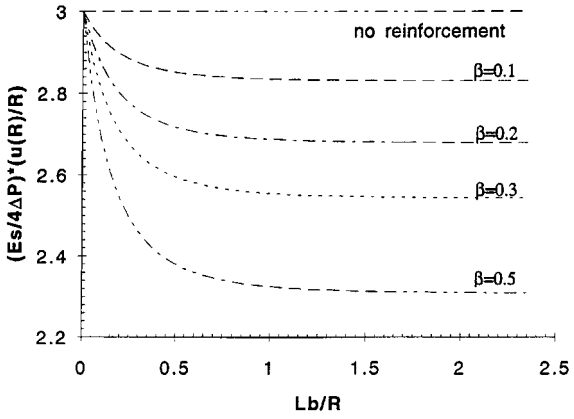

Figure 6. Dimensionless convergence vs. L_b/R for different values of β.

(2) the extrusion displacement of the front $U^* = (E_s/C)(u(R)/R)$, which occurs when $P_i = 0$ (i.e. when $\Delta P = P^*$).
(3) the maximum bolt tension $T_b^* = T_b\,(d_b/C)$.

7.4.1. Frontal displacement and extension of decompressed zone

Figures 7 and 8 show the dependence of the extent of the decompressed zone, on the normalized geostatic pressure $P^* = P_\infty/C$, for $\beta = 0{\cdot}5$ and for two particular values of $\Omega : \Omega = \infty$ (bolts indefinitely elastic) and $\Omega = 3$, while Figures 9 and 10 show the corresponding variations of the frontal displacement for the same set of parameters.

The following observations can be drawn:

(1) For linear elastic behaviour (absence of plastic zone with $W = w/R$ taken to be 1), the frontal displacement U^* varies linearly with the geostatic pressure P^*. In this region, the influence of bolts, for an already high stiffness contribution ($\beta = 0{\cdot}5$), is marginal, and little sensitive to variations of bolt lengths.
(2) Outside the elastic region, a largely non-linear displacement–loading relation shows up (Figures 9 and 10), and the importance of bolt length begins to appear. For $\beta = 0{\cdot}5$, $\Omega = 3$, $P^* = 5$ (Figure 10), doubling the bolt length from $0{\cdot}25R$ to $0{\cdot}5R$ reduces the convergence from $U^* = 7$ to 5 ($\sim$ 30 per cent reduction), while a still higher reduction can be expected at higher overburden.
(3) It is most interesting to note that, in all cases, the 'gain' from an increase in bolt length slows down drastically beyond $0{\cdot}5R$. Taking the same example as above, a further increase of L_b from $0{\cdot}5R$ to R (twice the above increment) only leads to a displacement reduction of 7 per cent (a quarter of the above), in other words eight times less efficient!

This remark is more clearly illustrated by Figures 11–14 where the variations of W and U^* are plotted directly against the bolt-length parameter b ($b = 1 + L_b/R$). Note that the curves largely flattens out for $b > 1{\cdot}5$, and are practically horizontal beyond $b = 2$ (i.e. no gain for bolt length larger than the radius R).

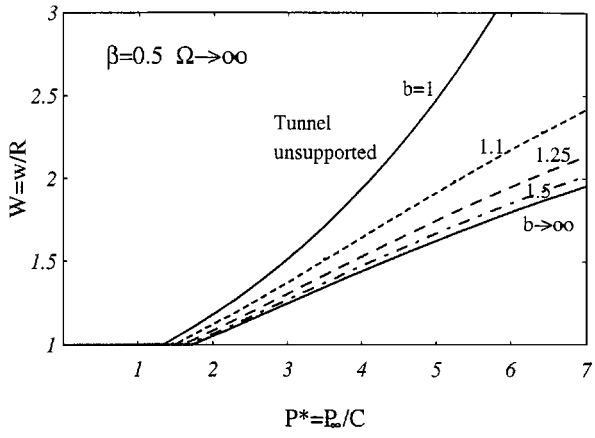

Figure 7. Plastic boundary W vs. overburden P^*, for $b = 1, 1{\cdot}1, 1{\cdot}25, 1{\cdot}5, \infty, \beta = 0{\cdot}5, \Omega = \infty$.

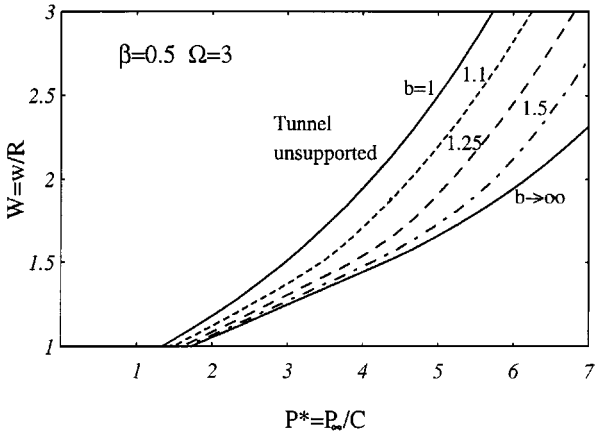

Figure 8. Plastic boundary W vs. overburden P^*, for $b = 1, 1{\cdot}1, 1{\cdot}25, 1{\cdot}5, \infty, \beta = 0{\cdot}5, \Omega = 3$.

It can also be observed that the influence of Ω (the strength contribution of bolts) is above-all sensitive for small bolt lengths. Beyond $b = 2$, the two cases $\Omega = 2$ and ∞ give practically the same result. In Figures 12 and 14, the two curves corresponding to $\beta = 0{\cdot}2$ and $0{\cdot}5$ and $\Omega = 2$ overlap for $b < 1{\cdot}25$ (i.e. $L_b < 0{\cdot}25R$) because in such cases yielding of bolts occurs over their entire length, and their contribution is therefore identical despite their unequal stiffness.

The last, but not the least important observation is the *absence of discontinuity* when the decompressed zone extends beyond the bolt length (i.e. when W bypasses b). For example, when W sweeps across the critical value $b = 1{\cdot}5$ at $P^* = 4{\cdot}1$ for $\beta = 0{\cdot}5$ and $\Omega = 3$ (Figure 8), the corresponding variation of the convergence U^*, which attains approximately $U^* = 3{\cdot}2$ (Figure 10), appears perfectly smooth at that point (with no 'kink'). The same continuity can also be

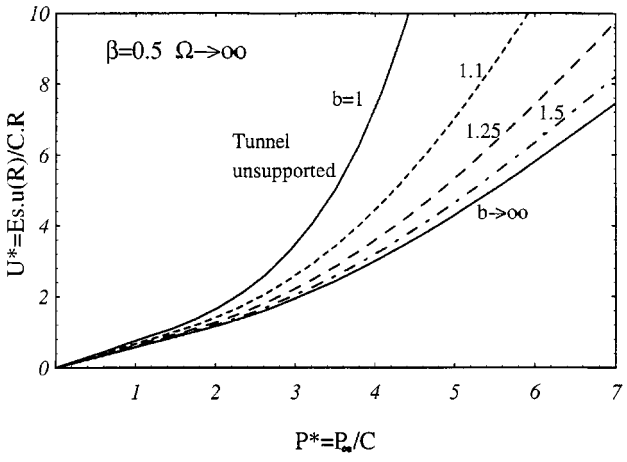

Figure 9. Convergence U^* vs. overburden P^*, for $b = 1, 1{\cdot}1, 1{\cdot}25, 1{\cdot}5, \infty, \beta = 0{\cdot}5, \Omega = \infty$.

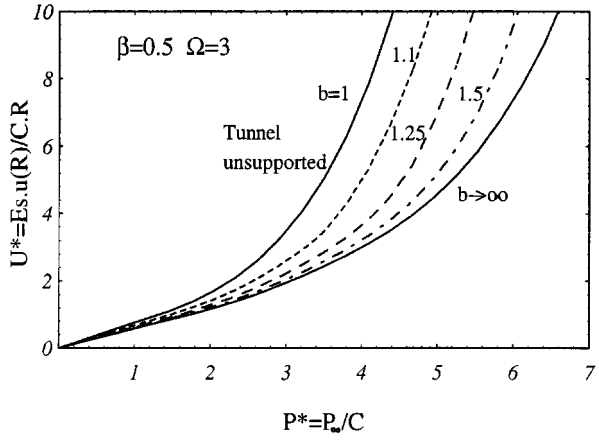

Figure 10. Convergence U^* vs. overburden P^*, for $b = 1, 1{\cdot}1, 1{\cdot}25, 1{\cdot}5, \infty, \beta = 0{\cdot}5, \Omega = 3$.

observed in Figures 11 and 12 where the event $W = b$ corresponds to intersections between the dotted diagonal and the family of curves. Note that the continuity of the function $W(P^*)$ implies that of $U^*(P^*)$ as they are related by the formula $U^* = W$.[3]

7.4.2. *Bolt tension*

The study of the variation of the maximum bolt tension as a function of P^*, β, Ω and b is the object of Figures 15–18, presented here below.

Figure 15 shows the stress build-up due to an increase of overburden, for the particular values of $\beta = 0{\cdot}5$ and $\Omega = \infty$. Again, any increase of bolt length beyond $L_b = R$ appears to be entirely inefficient.

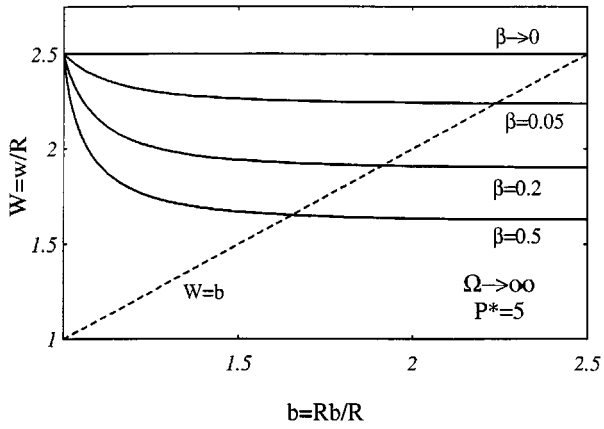

Figure 11. Plastic boundary W vs. bolt-length parameter b, for $\beta = 0, 0{\cdot}05, 0{\cdot}2, 0{\cdot}5, \Omega = \infty$, $P^* = 5$.

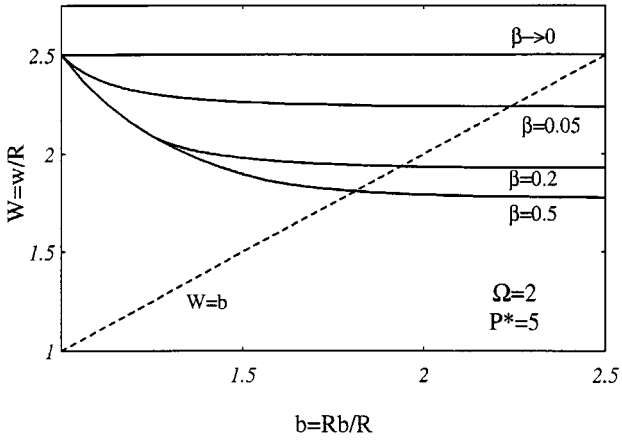

Figure 12. Plastic boundary W vs. bolt-length parameter b, for $\beta = 0, 0{\cdot}05, 0{\cdot}2, 0{\cdot}5, \Omega = 2$, $P^* = 5$.

The influence of bolt-strength on the tension build-up follows a very simple pattern, as shown in Figure 16. Before yielding occurs, bolt tension T_b^* is independent of Ω, hence the different curves corresponding to $\Omega = 2$, 4 and 6 overlap in this region. Once the yield limit is reached, bolt tension stagnants at its ultimate tensile strength T_{yb}, which explains the horizontal plateaus corresponding to $T_b^* = \Omega$. The set of curves plotted for $\Omega = \infty$ can therefore be used for any arbitrary value of Ω—it suffices to 'chop-off' horizontally at the given value of Ω.

In practice, for security reasons and due to uncertainties involved, practical bolt lengths for the frontal reinforcement are most of the time superior to the radius R. Having demonstrated that the overall behaviour is independent of bolt lengths for $L_b > R$ (i.e. $b > 2R$), it makes sense to study the case $b \to \infty$, which does possess some convenient simplifications, and allows to draw interesting conclusions out of this limiting case.

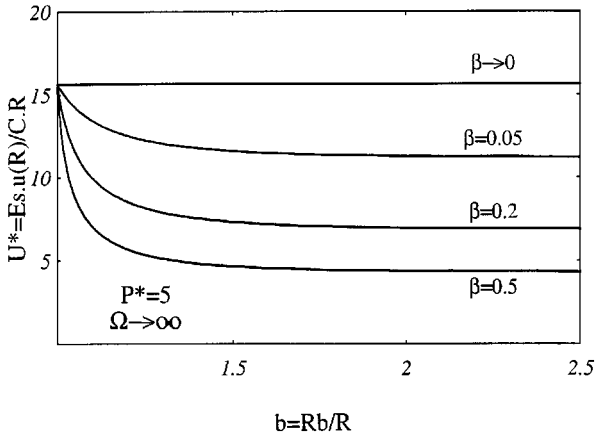

Figure 13. Convergence U^* vs. bolt-length parameter b, for $\beta = 0, 0{\cdot}05, 0{\cdot}2, 0{\cdot}5, \Omega = \infty$, $P^* = 5$.

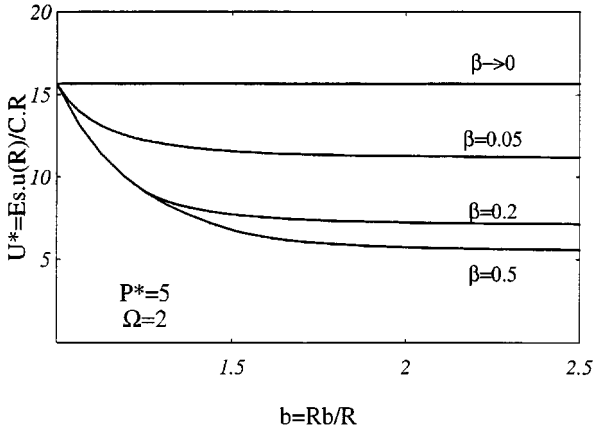

Figure 14. Convergence U^* vs. bolt-length parameter b, for $\beta = 0, 0{\cdot}05, 0{\cdot}2, 0{\cdot}5, \Omega = 2$, $P^* = 5$.

More often, for a given project with a predefined 'target depth', P^* is a known parameter and it is rather the 'reinforcement parameters' β and Ω which are to be decided by the designer. In regard to this last consideration, the dependence of bolt tension T_b on β and Ω is better illustrated by Figures 17–19.

For a fixed overburden P^* (the loading), the bolt tension T_b^* rises with β following the curve ($\Omega \to \infty$ in Figure 17, until the ultimate tensile strength is reached (i.e. when $T_b^* = \Omega$), after which the bolt tension stagnants (for ductile materials) or breaks (for brittle materials such as fibre glass). In the latter case, the designed bolt tension has to be limited to a certain percentage of its ultimate value, or in other words $\Omega/T_b^* = F > 1$.

The variation of T_b^* with respect to Ω for given values of P^* and β, as shown in Figure 18, is more subtle to interpret. Actually, for values of Ω above a certain threshold, the loading

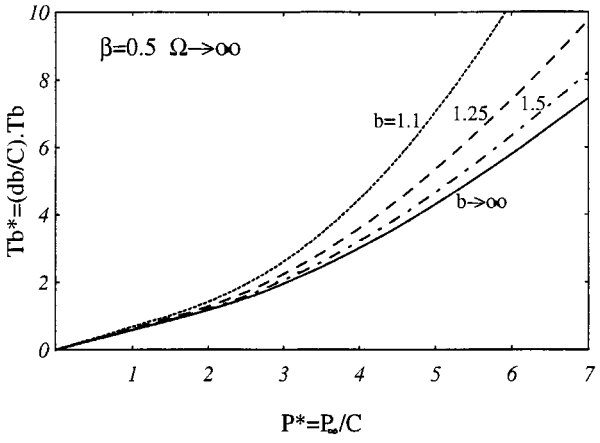

Figure 15. Bolt tension T_b^* vs. overburden P^*, for $b = 1, 1{\cdot}1, 1{\cdot}25, 1{\cdot}5, \infty, \beta = 0{\cdot}5, \Omega = \infty$.

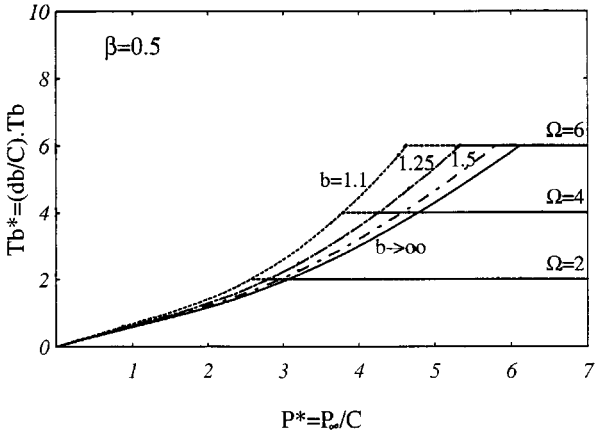

Figure 16. Bolt tension T_b^* vs. overburden P^*, for $b = 1, 1{\cdot}1, 1{\cdot}25, 1{\cdot}5, \infty, \beta = 0{\cdot}5, \Omega = 2, 4, 6$.

parameter P^*, taking account of the relative bolt stiffness β, does not create any yielding inside the bolts. This explains the independence of T_b^* with respect to Ω, and the horizontal plateaus (the 'elastic lines') to the right. Moreover, curves at high values of β are above those at lower values of β, since stiffer bolts tend to attract a higher proportion of loading.

For values of Ω below the aforementioned threshold (i.e. ultimate tensile strength of bolt below a certain value), yielding takes place at least over part of the bolt-length close to the front. In the latter case, the maximum bolt tension is necessarily equal to its ultimate tensile strength (i.e. $T_b^* = \Omega$), which explains the diagonal 'plastic line' towards which all the horizontal 'elastic lines' tend.

Finally, Figure 19 presents a three-dimensional view of the surface $T_b^* = T_b^*(\beta, \Omega, P^* = 5)$ of which Figures 17 and 18 are just the 'side views'.

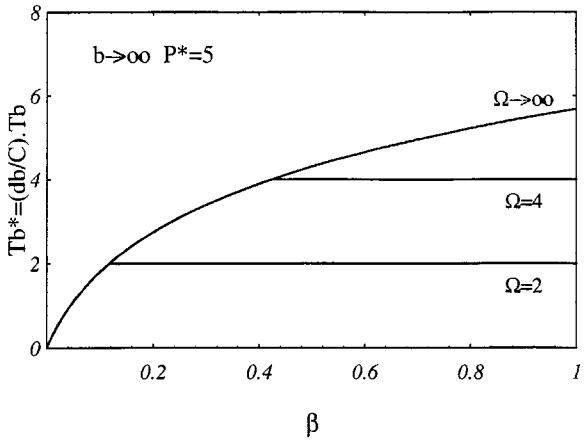

Figure 17. Bolt tension T_b^* vs. stiffness contribution β, for $\Omega = 2, 4, \infty, b = \infty, P^* = 5$.

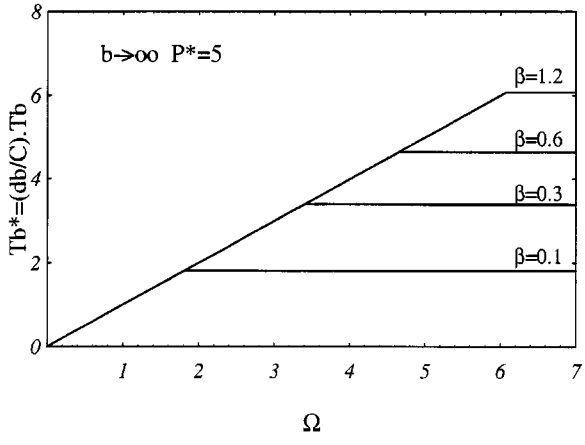

Figure 18. Bolt tension T_b^* vs. strength contribution Ω, for $\beta = 0{\cdot}1, 0{\cdot}3, 0{\cdot}6, 1{\cdot}2, b = \infty, P^* = 5$.

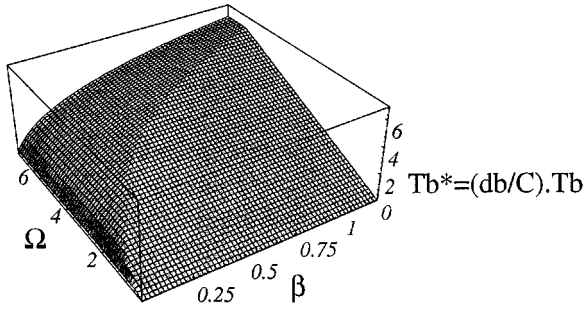

Figure 19. Bolt tension T_b^* vs. stiffness contribution β and strength contribution Ω, for $b = \infty$ and $P^* = 5$.

8. VERIFICATION OF THE ANALYTICAL MODEL

In order to investigate the precision of its predictions, the analytical solution has been compared to a numerical approach. The analysis[11] has been carried out using a three-dimensional finite difference code (FLAC 3D[26,27]), which allows to take into account the 'exact' geometry of the tunnel, among others the lining behind the face and the non-linearities of the behaviour, in particular the imperfect bonding between bolt and ground. The tunnel is considered to be at great depth, and the initial stress field is supposed to be homogeneous and isotropic. As a consequence of the symmetry, only a quarter of the geometry is considered and each bolt, parallel to the tunnel axis, is modelled individually. The difference in bolt arrangement between the numerical method (Figure 20) and the analytical model (Figure 2) has already been commented in paragraph 1 during the introduction of the spherical symmetry assumption.

In the comparative study presented hereafter, the geometry as well as the geotechnical parameters considered, based on *in situ* measurements, are those adopted for the design of the cross-town tunnel in Toulon (France). The model is that of a circular tunnel of radius $R = D/2 = 5{\cdot}80$ m, in a deep and isotropic ground, modelled as an elastic–perfectly plastic material obeying Tresca's yield criterion and its associated flow rule. In the numerical model, the lining support behind the face (shotcrete) is linear elastic and is installed up to the tunnel face simultaneously with excavation step. This sequence of work is equivalent to pre-vaults executed ahead of the face.[28] Geomechanical parameters for soil and shotcrete lining are summarized in Table VI.

The bolts are modelled as linear elements of elastic–perfectly plastic behaviour with a fixed yield strength (Table VI). In order to simulate perfect bonding (e.g. grouting) in the same way as in the analytical approach, rheological parameters at interface between fibre-glass bolts and soil are: shear stiffness 2×10^9 kN and maximum shear force 1×10^6 kN/ml. Excavation has been simulated in 12 steps of 3 m: at the beginning, each bolt has a length of 10 times the tunnel diameter ($L_0 = 10D$), the maximum allowed by the mesh boundary. For each excavation step and for each bolt, a segment of 3 m is removed from the model, therefore after n excavations we have bolts of length $L_n = (10D - 3n)$ in meters. The 'degree' of reinforcement can, however, be considered constant despite this length reduction, since it has been shown[11] that no significant increase of performance can be observed by increasing bolt length beyond 9 m. In other words, at each stage of excavation, the real length is largely beyond the critical area, so that they can be considered as infinite in the numerical calculations. Although the influence of bolt length has not been studied in the following comparison, it seems that the analytical solution underestimates the minimum critical bolt length, since in the numerical approach, bolt tension is negligible beyond

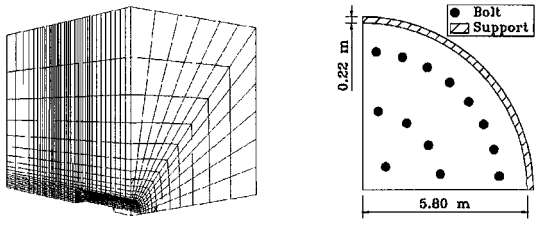

Figure 20. 3D mesh and bolt distribution at the face (52 for a full face) of the numerical model.

Table VI. Soil mass, shotcrete lining and bolts properties

Parameters	Soil mass	Concrete lining	Fibre-glass bolts
Elastic modulus E (MPa)	300	10000	20000
Poisson's ratio ν	0·3	0·2	†
Density γ (kg/m^3)	2350	2500	†
Cohesion C (MPa)	0·200	†	†
Thickness (m)	†	0·22	†
Yield strength σ_{yb} (MPa)	†	†	500
Section S_b (mm^2)	†	†	1500

† Not applicable

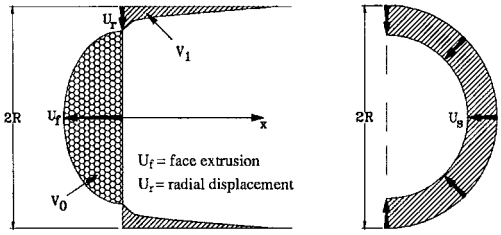

Figure 21. Face configuration for the numerical and the analytical approach.

1·5R, while for the analytical solution, bolt length increase layer than R does not give any significant effect (Figure 6).

In the comparative analysis, several values of the overburden and the bolt density have been considered: an elastic case with an overburden $P_\infty = 1{\cdot}2$ MPa (case EL), and three plastic cases with $P_\infty = 0{\cdot}8$, 1·2, 1·6 MPa (i.e. $P^* = P_\infty/C = 4, 6, 8$). As it is shown in Figure 21, the analytical approach models the front as a hemispherical surface ($S_{\text{ana.}} = 2\pi R^2 = 212$ m^2), twice the tunnel face area accounted for in the numerical approach ($S_{\text{num.}} = \pi R^2 = 106$ m^2). In order that the bolts take the same working force, both models take into account the same number of bolts at the face. As a consequence, 'bolt density' in the analytical approach is half the value in the numerical approach. In the following paragraphs, the bolt density d_b will mean the bolt density in the numerical approach: 0, 20, 52 and 160 bolts at the face (i.e. $d_b = 0$, 0·2, 0·5, 1·5 bolts/m^2).

A small number of important design parameters have been studied: extrusion volume at the face, average frontal displacements and bolt tension. A more complete comparative study can be found in another publication.[29]

8.1. Extrusion volume and average extrusion movement

For each model, extrusion volume is calculated as follows (Figure 21):

in the numerical model: $V_{\text{num.}} = V_0$ is the integration of U_f on the front face ($S = \pi R^2$),

in the analytical model: $V_{\text{ana.}} = U_s 2\pi R^2$, since the frontal displacement is uniform.

Figure 22 represents the evolution of the ratio $V_{\text{num.}}/V_{\text{ana.}}$ according to the number of bolts at the face. In the elastic case (EL), this ratio remains constant: $V_{\text{num.}}/V_{\text{ana.}} = 0{\cdot}55$. For realistic

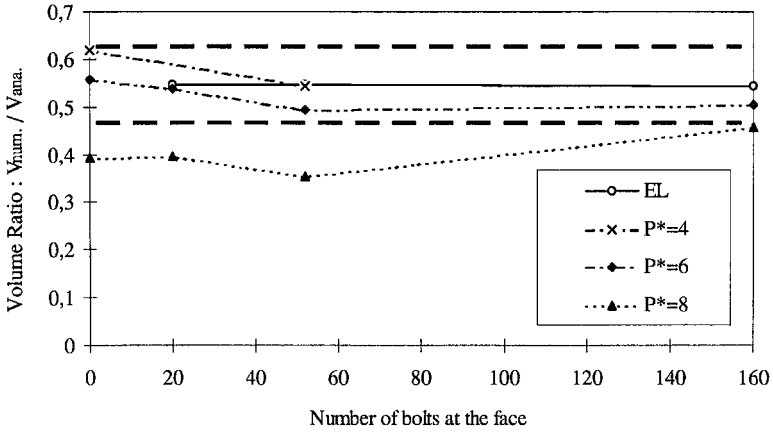

Figure 22. Extrusion volume ratio vs. the number of bolts at the face ($d_b = 0{\cdot}5$ bolt/m^2).

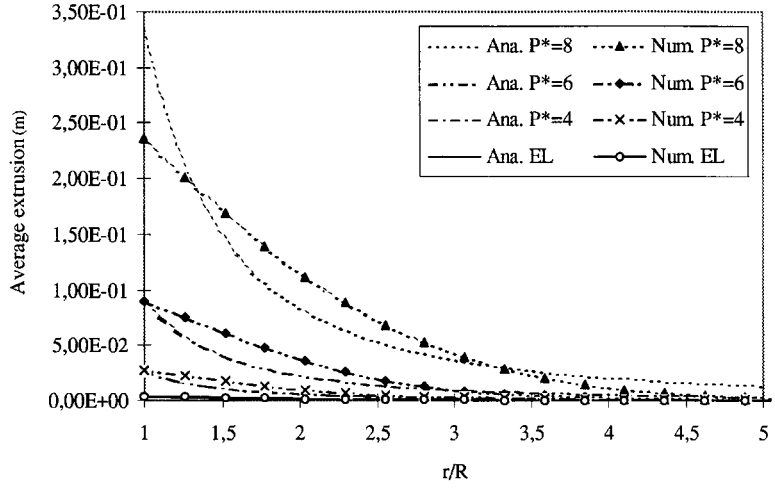

Figure 23. Average extrusion movement vs. distance from the face.

values of overburden ($P^* = 4$ or 6), the ratio lies inside the interval $0{\cdot}50 < V_{\text{num.}}/V_{\text{ana.}} < 0{\cdot}60$, for a large range of bolt density. For $P^* = 8$, the ratio is closer to 0·40. However, this level of overburden characterizes situations close to failure: Broms and Bennermark[30] have proposed the criterion $P^* < 6$–7 in order to ensure the stability of the cavity. Hence, the validity of the results obtained for the case $P^* = 8$ is very doubtful.

Taking into account the fact that the hemispherical front is twice the real face area, we can conclude that the analytical model gives a good approximation of the average extrusion movement at the face. This last quantity is plotted in Figure 23 against the distance from the face ($r/R = 1$ at the front, and increases beyond the face), considering a bolt density $d_b = 0{\cdot}5$ bolt/m^2. As mentioned previously, the average displacement at the front is correctly estimated by the

Table VII. Dimensionless average extrusion movement at the face vs. overburden

	U^*								
	EL			$P^* = 4$			$P^* = 6$		
db (b/m2)	Ana.	Num.	Diff. (%)	Ana.	Num.	Diff. (%)	Ana.	Num.	Diff. (%)
0	1·00	†	†	7·39	9·13	23·6	33·12	36·93	11·5
0·2	0·99	1·09	9·3	7·10	†	†	28·63	30·86	7·8
0·5	0·99	1·08	9·4	6·68	7·28	9·0	23·66	23·30	− 1·5
1·5	0·96	1·04	8·6	5·70	†	†	16·01	16·20	1·2

† Not calculated

analytical approach, but it decreases more rapidly away from the tunnel face than in the numerical model. For $P^* > 7$, results from the two models differ for the aforementioned reasons and we will not consider load factors $P^* > 7$, in the remaining sections.

Table VII shows the results of the two models for the normalized extrusion movement at the front in the elastic case and for realistic values of the load factor ($P^* \leqslant 6$). It can be observed that the displacements at the front given by the analytical model are close to the numerical results. The maximum difference between the two models reaches 24 per cent, for all cases considered. This level of precision is acceptable for preliminary design purposes.

8.2. Bolt tension

Concerning the bolt tension, the shapes of the curves (Figure 24) from the two models are strongly different. In the analytical model, bolt tension is largely overestimated at the tunnel face: when $P^* = 4$, the curves differ at the face due to skin effects, and for $P^* > 5$, bolts have yielded in the analytical approach whereas they remain elastic in the numerical one.

9. CONCLUSIONS

As a complement to 'stability' approaches, the analytical model proposed allows to estimate the extrusion movements ahead of the excavation front of a tunnel, as well as the extent of the decompressed zone, taking into account the progressive force build-up in the bolts, long after yielding of ground has taken place. Not only such information is important in order to estimate correctly the damage potential on nearby and surface structures, it is also by itself an indirect indication on the level of stability of the tunnel head. In the case of sensitive materials, the possible strength-loss due to decompression during excavation can eventually be assessed, leading to a refinement of the stability calculations.

In regard to the mechanical behaviour, the contribution of the bolts on the improvement of the mechanical characteristics of the ground, is represented in this model by two dimensionless parameters: β (the stiffness contribution) and Ω (the strength contribution). Bearing in mind that such improvements have a directional character, the homogenization approach leads to an overall anisotropic behaviour. The effect of the progressive build-up of bolt tension, directly

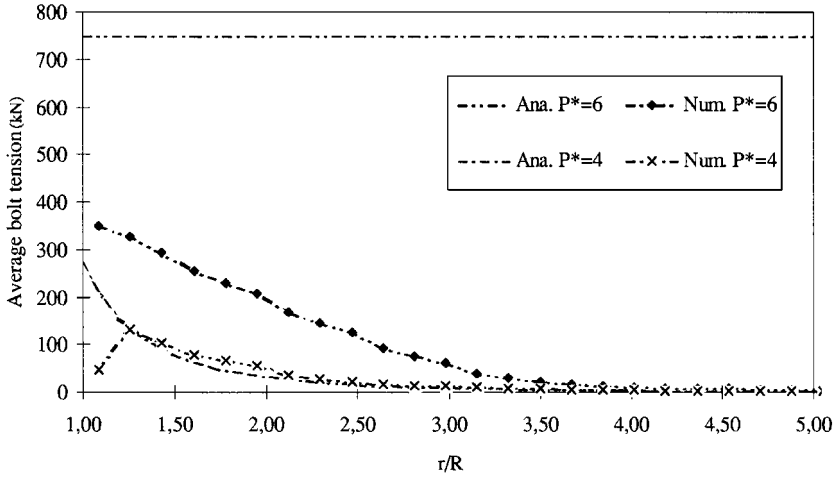

Figure 24. Average bolt tension vs. distance from the face ($d_b = 0{\cdot}5$ bolt/m^2).

visible from the dependence of the frontal displacement on bolt stiffness β, has been shown to be a determining factor. Design methods, which assume hypothetically that the bolts are working at a fixed percentage of their ultimate tensile strength, can therefore only be erroneous.

The influence of bolt-length has also been studied by introducing an additional parameter b, not accounted for in previous studies except under linear elastic behaviour.[14] Results of analyses seem to show that, firstly, bolt-lengths longer than R are inefficient, and secondly, contrary to common belief, there is no sudden 'jump' in the extrusion movement of the front when the decompressed zone sweeps across the end of the bolts and enters the unreinforced zone. Nonetheless, extreme caution must be taken here against any hasty conclusions, on account of the hypotheses involved—elastic incompressibility and perfect bonding amongst others. A finite bond strength, for example, leads logically to a finite anchorage length, which is all the more important as the bond strength is low. Further investigations, notably by experimental means, are therefore indispensable to arrive at a final conclusion.

From the utility standpoint, a variable count shows that, including the loading parameter P^*, which is actually the normalized geostatic pressure, the structural behaviour only depends on four dimensionless parameters (β, Ω, b and P^*), hence the model possesses a great simplicity. This makes the model ideally suited to quantity estimations and parametric studies at the preliminary design stage. As a matter of fact, the parametric studies presented constitute already in itself a very useful design aide. The explicit character of the equations—such as those governing the evolution of the plastic boundaries, or the elastic limit $\Delta P^{*(1)}$—also allows one to visualize the different events. On the other hand, the simplifying assumptions do put limits on the range of validity of the model. Hence, in order to appreciate the precision of the analytical model, its results are compared to those obtained by a numerical model (FLAC 3D). For values of the load factor below $P^* = 6$, the maximum difference on the extrusion movement amounts to 24 per cent, and appears to be an acceptable value for practical preliminary design applications. Although the precision of the model drops for load factors $P^* \geqslant 8$, the feasibility of such cases in practice is questionnable: the studies by Broms and Bennermark[30] showed that the failure is probable and large movements, probably beyond acceptable limits, are to be expected in such cases.

In addition to the partial validation of the model presented in this paper, other comparisons were performed with *in situ* measurements from the tunnel of Tartaiguille[5] (Table I) which showed very good agreement between field data and the theoretical results.[31] The analytical developments were built in a computer code[32] written in C^{++}, with built-in graphic facilities and interactive input/output, to allow quick design calculations to be performed. The present version includes yield criteria of Tresca or Coulomb type, strain softening behaviour is currently being implemented. Another approach is under progress in order to assess the stability conditions of the reinforced face, using theoretical computations as well as laboratory experiments.[33] Hence, the model proposed here forms part of a long-term research project, which aims at constituting a knowledge base for the conception and design of localized reinforcement in the form of linear inclusions in underground works.

ACKNOWLEDGEMENT

Part of this research was sponsored by the French National Tunneling Research Center (Centre d'Etudes des Tunnels, CETU). The authors also appreciate the interesting discussions with P. Dubois of CETU.

APPENDIX I

RESOLUTION PROCESS FOR EACH CONFIGURATION

To fix ideas, we will treat the configurations in the order 1–5, as encountered in Case A (Figure 4(a)), followed by the Configuration 6 in Case B (Figure 4(b)). Attention will be concentrated on the determination of the plastic boundaries—the fundamental unknowns of the problem, as well as the critical values of the loading parameter ΔP, which defines the transition from one configuration to another.

Configuration 1 (*Soil and bolts elastic everywhere*): In an elastic zone (Figure 25), the plastic strain ζ is identically zero, we are thus left with three unknowns with three equations (6)–(8). The displacement u is given by expression (11). Back substitution into (7) and elimination of σ_θ from (8) leads to the following differential equation on σ_r:

$$\frac{\partial \sigma_r}{\partial r} + \frac{4E_s B}{r^4}\left[1 + \frac{k^2}{r^2}\right] = 0 \tag{12}$$

which admits the following general solution:

$$\sigma_r = -P_\infty + 4BE_s\left[\frac{k^2}{5r^5} + \frac{1}{3r^3}\right] + D \tag{13}$$

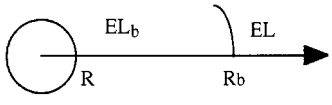

Figure 25. Configuration 1: EL = elastic unbolted, EL$_b$ = elastic bolted.

Table VIII. Detailed solution for Configuration 1

	EL_b $(R < r < R_b)$	EL $(R_b < r < \infty)$
u	$-\dfrac{B}{r^2}$ with $B = \dfrac{\Delta P}{4E_s}\left[\dfrac{k^2}{5}\left(\dfrac{1}{R^5} - \dfrac{1}{R_b^5}\right) + \dfrac{1}{3R^3}\right]^{-1}$	
σ_r	$-P_\infty + 4E_sB\left[\dfrac{k^2}{5r^5} + \dfrac{1}{3r^3}\right] - 4E_sB\dfrac{k^2}{5R_b^5}$	$-P_\infty + \dfrac{4}{3}E_s\dfrac{B}{r^3}$
σ_θ	$-P_\infty - E_sB\left[\dfrac{6k^2}{5r^5} + \dfrac{2}{3r^3}\right] - 4E_sB\dfrac{k^2}{5R_b^5}$	$-P_\infty - \dfrac{2}{3}E_s\dfrac{B}{r^3}$

where D is a constant of integration independent of r. In the outer unreinforced zone ($r > R_b$), $k = 0$, while the boundary condition $\sigma_r(r \to \infty) \to -P_\infty$ implies $D = 0$, hence we deduce that

$$\sigma_r = -P_\infty + \frac{4BE_s}{3r^3} \tag{14}$$

In the inner reinforced zone, the general solution (13) applies. Continuity of radial stress at R_b allows to express D in terms of B:

$$D = -\frac{4E_sBk^2}{5R_b^2} \tag{15}$$

while the boundary condition $\sigma_r(R) = -P_i$ gives

$$B = \frac{\Delta P}{4E_s}\left[\frac{k^2}{5}\left(\frac{1}{R^5} - \frac{1}{R_b^5}\right) + \frac{1}{3R^3}\right]^{-1} \tag{16}$$

The problem is thus completely solved, the detailed solution is given in Table VIII. Note that this configuration is valid only if the yield criterion is nowhere reached.

When yielding occurs, either for the ground or for the bolts, the solution of Configuration 1 ceases to apply. In case where the yield strain of bolts is higher than that of the ground, yielding of the latter will take place first. An examination of realistic parameters shows that this is always the case, and hence will be assumed throughout this paper. As both the bolt density and the stress intensity decreases with radius, yielding does not necessarily begin at $r = R$. Substitution of the expressions of σ_r and σ_θ (Table VIII) into (2), using the form (3) for $\sigma_0(r)$ in the zone EL_b and zero in EL, it can be shown that the yield criteria in both zones reduce to the same expression below:

$$F(\boldsymbol{\sigma}, r) = \frac{2E_sB}{r^3} - 2C \tag{17}$$

Since F is monotone decreasing in r, yielding must first occur at the front ($r = R$), which happens when B takes the value of $(C/E_s)R^3$, leading to the following critical value of the loading

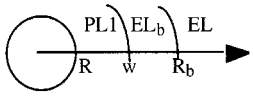

Figure 26. Configuration 2: PL1 = medium yielded, bolts elastic.

parameter ΔP:

$$\frac{\Delta P^{(1)}}{C} = \frac{4}{3}\left\{1 + \frac{3}{5}\beta[1 - b^{-5}]\right\} \tag{18}$$

where $b = R_b/R$ is another important dimensionless parameter characterizing the effect of bolt length.

Configuration 2: For the elastic zones (Figure 26) EL and EL_b, the expression in the Table VIII remain valid, but the parameter B takes a different value here since the zone EL_b is no longer in contact with the front $r = R$. Instead, the yield condition at $r = w^+$ leads to

$$B = \frac{C}{E_s} w^3 \tag{19}$$

In the plastic zone PL1, eliminating σ_θ from the equilibrium equation (8) and the yield criterion (3), taking into account the form of ε_r in (11) leads to the following differential equation on σ_r:

$$r\frac{\partial \sigma_r}{\partial r} + 4C + 4E_s B\frac{k^2}{r^5} = 0 \tag{20}$$

Radial stress continuity on w and the form (19) of B then lead to

$$\sigma_r = -P_\infty + \frac{4C}{3} + 4C\,\mathrm{Ln}\left(\frac{w}{r}\right) + \frac{4Ck^2}{5}\left(\frac{1}{r^5} - \frac{1}{R_b^5}\right) w^3 \tag{21}$$

The last unknown w can be determined by applying the boundary condition $\sigma_r(R) = -P_i$, which results in the following non-linear algebraic equation:

$$\Delta P^* = \tfrac{4}{3} + 4\,\mathrm{Ln}\,W + \tfrac{4}{5}\beta[1 - b^{-5}]W^3 \tag{22}$$

where $W = w/R$, and $\Delta P^* = \Delta P/C$, b and β having already been defined. It is readily seen that the right-hand side of the above equation starts with the value of $\Delta P^{*(1)}$ (less than ΔP^*) at $W = 1$ and increases monotonously to positive infinity. The above equation admits therefore a unique solution of W, and solves completely the problem.

Two different conditions can independently mark the end of validity of Configuration 2:

Case A: Bolts start to yield in PL1, firstly at $r = R$.

Case B: Radius w reaches R_b, and penetrates into the unreinforced soil mass beyond radius R_b.

For Case A, the condition $\varepsilon_r(R) = 2B/R^3 = \varepsilon_{yb}$, combined with (19), simplifies to $W^3 = \varepsilon^* = E_s\sigma_{yb}/2E_bC$. Substituting this particular value of W into equation (22) leads to the

Table IX. Detailed solution for Configuration 2

	PL1 ($R < r < w$)	EL & EL_b ($w < r < \infty$)
u	$-\dfrac{B}{r^2}$ with $B = \dfrac{C}{E_s} w^3$	
σ_r	$-P_\infty + \dfrac{4C}{3} + 4C\,\mathrm{Ln}\left(\dfrac{w}{r}\right) + \dfrac{4Ck^2}{5}\left(\dfrac{1}{r^5} - \dfrac{1}{R_b^5}\right) w^3$	Formally identical to expressions in Table VIII, but with $B = \dfrac{C}{E_s} w^3$
σ_θ	$-P_\infty - \dfrac{2C}{3} + 4C\,\mathrm{Ln}\left(\dfrac{w}{r}\right) - \dfrac{2Ck^2}{5}\left(\dfrac{3}{r^5} + \dfrac{2}{R_b^5}\right) w^3$	
ζ	$\dfrac{2C}{E_s}\left[\dfrac{w^3}{r^3} - 1\right]\left[1 + \dfrac{k^2}{r^2}\right]^{-1}$	

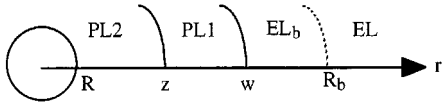

Figure 27. Configuration 3: PL1 = medium yielded, bolts elastic. PL2 = both yielded.

following critical value of ΔP:

$$\Delta P^{*(2A)} = \tfrac{4}{3} + \tfrac{4}{3}\,\mathrm{Ln}(\varepsilon^*) + \tfrac{4}{5}\beta[1 - b^{-5}]\varepsilon^* \tag{23}$$

For Case B, putting $W = b$ into equation (22) we get

$$\Delta P^{*(2B)} = \tfrac{4}{3} + \tfrac{4}{3}\,\mathrm{Ln}(b^*) + \tfrac{4}{5}\beta[1 - b^{-5}]b^3 \tag{24}$$

It is easily seen that if $\varepsilon^* < b^3$, then $\Delta P^{*(2A)} < \Delta P^{*(2B)}$, and bolts start to yield at $r = R$ before the plastic radius w reaches R_b (Case A), and vice versa (Case B). The two possible evolutions are presented in Figure 4. We will continue the analysis here for Case A.

Configuration 3: The expressions in Table IX remain valid for the three outer zones since their determination does not involve the boundary condition at $r = R$, except that the unknown radius w is not determined by equation (22), due to the presence of PL2 (Figure 27). This time, the yield criterion (3) at w^+ gives

$$\left(\frac{w}{z}\right)^3 = \varepsilon^* \tag{25}$$

For the zone PL2, eliminating σ_θ from the equilibrium condition (8) and the yield criterion (4) gives

$$r\frac{\partial \sigma_r}{\partial r} + 4C + 2\frac{k^2}{r^2}\frac{E_s}{E_b}\sigma_{yb} = 0 \tag{26}$$

Table X. Detailed solution for Configuration 3

	PL2	PL1, EL_b, EL
u	$-\dfrac{B}{r^2}$ with $B=\dfrac{C}{E_s}w^3$	
σ_r	$-P_i+4C\,\mathrm{Ln}\left(\dfrac{R}{r}\right)+2C\varepsilon^*\left[\dfrac{k^2}{r^2}-\dfrac{k^2}{R^2}\right]$	Formally identical to expressions in Table IX
σ_θ	$-P_i-(2+\Omega)C+4C\,\mathrm{Ln}\left(\dfrac{R}{r}\right)$	
ζ	$\left(\dfrac{2C}{E_s}\right)\left\{\dfrac{k^2}{r^2}\left[\dfrac{w^3}{r^3}-\varepsilon^*\right]+\dfrac{w^3}{r^3}-1\right\}\left[1+\dfrac{k^2}{r^2}\right]^{-1}$	

Its solution, on account of the boundary condition $\sigma_r(R)=-P_i$ writes

$$\sigma_r=-P_i+4C\,\mathrm{Ln}\left(\frac{R}{r}\right)+2C\varepsilon^*\left[\frac{k^2}{r^2}-\frac{k^2}{R^2}\right] \tag{27}$$

Finally, continuity of radial stress at $r=z$ leads after simplification to the following equation on the unknown w, which admits a unique solution, and solves at the same time completely the problem, with the detailed solution reported in Table X:

$$\Delta P^*=\frac{4}{3}+4\,\mathrm{Ln}\,W+\Omega\left[1-\frac{3}{5}\frac{\varepsilon^{*2/3}}{W^2}\right]-\frac{4}{5}\beta b^{-5}W^3 \tag{28}$$

This configuration ceases to apply when the plastic boundary w reaches R_b. Substitution of $W=b$ into equation (28) gives the corresponding critical value of ΔP:

$$\Delta P^{*(3)}=\frac{4}{3}+\frac{4}{3}\mathrm{Ln}(b^3)+\Omega\left[1-\frac{3}{5}\frac{\varepsilon^{*2/3}}{b^2}\right]-\frac{4}{5}\beta b^{-2} \tag{29}$$

Configuration 4: Relations (19) and (25) continue to apply (i.e. yielding of ground at w^+ and bolts at z^+). The stresses in the outer zone EL are given by (14) and (19), while in the zone PL3 (Figure 28) eliminating σ_θ from the equilibrium equation (8) and the yield criterion (2) with $\sigma_0(r)=0$, taking into account the continuity of radial stress on w, leads to

$$\sigma_r=-P_\infty+\frac{4C}{3}+4C\,\mathrm{Ln}\left(\frac{w}{r}\right) \tag{30}$$

The radial stresses in the plastic zones PL1 and PL2 are formally the same as in Configuration 3. Finally, the boundary condition $\sigma_r(R)=-P_i$ in PL2 leads to the desired equation on w:

$$\Delta P^*=\frac{4}{3}+4\,\mathrm{Ln}\,W+\Omega\left[1-\frac{3}{5}\frac{\varepsilon^{*2/3}}{W^2}\right]-\frac{4}{5}\beta b^{-5}W^3 \tag{31}$$

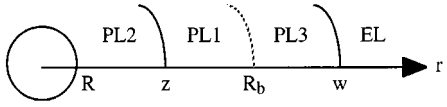

Figure 28. Configuration 4: PL3 = medium yielded (unreinforced).

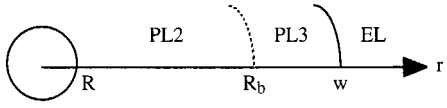

Figure 29. Configuration 5: entire length of bolts yielded.

Table XI. Detailed solution for Configuration 4

	PL2 & PL1	PL3	EL & EL_b
u		$-\frac{B}{r^2}$ with $B=\frac{C}{E_s}w^3$	
σ_r	Formally identical to expressions in Table X	$-P_\infty+\frac{4C}{3}+4C\,\mathrm{Ln}\left(\frac{w}{r}\right)$	Formally identical to expressions in Table X
σ_θ		$-P_\infty-\frac{2C}{3}+4C\,\mathrm{Ln}\left(\frac{w}{r}\right)$	
ζ		$\frac{2C}{E_s}\left[\frac{w^3}{r^3}-1\right]$	

The validity of this configuration ceases to hold when the plastic boundary z reaches R_b (i.e. when $W^3=\varepsilon^* b^3$). This occurs when

$$\Delta P^{*(4)}=\tfrac{4}{3}[1+\mathrm{Ln}(\varepsilon^* b)]+\Omega(1-b^{-2})-\tfrac{2}{5}\Omega b^{-2} \tag{32}$$

Configuration 5: The stresses and all other physical quantities in all three zones admit the same expressions as in Configuration 4 (Table XI), with $B=(C/E_s)w^3$, while a different value of w comes from the radial stress continuity at $r=R_b$ between PL2 and PL3 (Figure 29):

$$\Delta P^*=\tfrac{4}{3}+4\,\mathrm{Ln}\,\mathbf{W}+\Omega[1-b^{-2}] \tag{33a}$$

leading to an explicit solution of W:

$$W=\mathrm{Exp}\left[\frac{\Delta P^*}{4}-\left\{\frac{1}{3}+\frac{\Omega}{4}(1-b^{-2})\right\}\right] \tag{33b}$$

This configuration holds all the way up to $\Delta P=P_\infty$, when the internal pressure reaches zero.

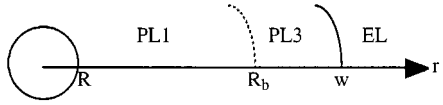

Figure 30. Configuration 6.

Configuration 6: Expressions for the field quantities (Figure 30), in particular the stresses, are given in Table XI for zones PL3 and EL (integration from ∞ to r), and by Table X for the plastic zone PL1 (integration from R to r). Radial stress continuity leads to the equation on w, which turns out to be identical to that of Configuration 2.

The transition value of ΔP^* between Configurations 6 and 4, resulting from the yield condition of bolts on $r = R$, is found to admit the same expression as $\Delta P^{*(2A)}$, while the transition value between Configuration 2 and 6 is equal to $\Delta P^{*(2B)}$ as mentioned previously.

APPENDIX II. NOTATION

E_s, C, ν_s	Young's modulus, cohesion and Poisson's coefficient ($\nu_s = 0{\cdot}5$) of ground
λ_s, μ_s	Lamé's coefficients of ground, related to E_s and ν_s by $\lambda_s = \nu_s E_s/[(1+\nu_s)(1-2\nu_s)]$, $\mu_s = E_s/[2(1+\nu_s)]$
S_b, d_b	section (m^2) and density (number of bolts/m^2 at tunnel head) of bolting
E_b, σ_{yb}	Young's modulus and yield stress of bolts
$\beta = d_b S_b E_b/E_s = \Delta E/E_s$	dimensionless parameter characterizing the stiffness contribution of bolts
$\Omega = d_b S_b \sigma_y/C = \Delta C/C$	dimensionless parameter characterizing the strength contribution of bolts
$k = \sqrt{\beta}\, R$	
$\varepsilon_{ys} = 2C/E_s$, $\varepsilon_{yb} = \sigma_{yb}/E_b$	yield strains of ground and of bolts
$\varepsilon^* = \varepsilon_{yb}/\varepsilon_{ys} = \Omega/2\beta =$ $(\sigma_{yb}/2C)(E_b/E_s)$	($\varepsilon^* > 1$ assumed)
R	radius of spherical front
L_b, $R_b = R + L_b$, $b = R_b/R$	bolt length, outer boundary of the reinforced zone and its normalized value
$\Delta P = P_\infty - P_i$, ΔP^* $= \Delta P/C$	dimensional and dimensionless mechanical loading parameter
w, z, $W = w/R$, $Z = z/R$	outer and inner plastic boundaries and their normalized counterparts
ζ	plastic radial strain (i.e. $\varepsilon^P_{rr} = \zeta$, $\varepsilon^P_{\theta\theta} = \varepsilon^P_{\phi\phi} = -\zeta/2$), characterizing completely the plastic strain tensor
T_b, T_{yb}	tensile force ($0 < T_b < T_{yb}$) and the failure load ($T_{yb} = S_b \sigma_{yb}$) of bolts
$\sigma_0(r)$	homogenized radial stress due to bolts ($\sigma_0(r) = d_b T_b(R^2/r^2)$)
σ_b	tensile stress in bolts ($\sigma_b = T_b/S_b$)
$\boldsymbol{\sigma}_b$	homogenized uniaxial stress tensor ($\boldsymbol{\sigma}_b = \sigma_0(r)\, \mathbf{e}_r \otimes \mathbf{e}_r$)

REFERENCES

1. Pelizza S, Peila D. Soil and rock reinforcements in tunneling. *Tunnelling Underground Space Technology* 1993; **8**(3): 357–372.
2. Lunardi P. Fiber-glass tubes to stabilize the face of tunnels in difficult cohesive soils. *SAIE—Seminar. The Application of Fiber Reinforced Plastics (FRP) in Civil Structural Engineering*, Bologna, Italy, 1993.
3. Lunardi P, Focaracci A, Giorgi P, Papacella A. Tunnel face reinforcement in soft ground design and controls during excavation. *Proceedings of International Conference Towards New Worlds in Tunnelling*, vol. 2, Acapulco, 16–20 May 1992; 897–908.
4. Lunardi P. Conception et exécution des tunnels d'après l'analyse des déformations contrôlées dans les roches et dans les sols: présoutènement et préconfinement, *Revue Française de Géotechnique*, 1997; **80**:17–34.
5. EMMC. Tartaiguille: une nouvelle méthode. *Tunnels et Ouvrages Souterrain* 1998; **145**:29–31.
6. Peila D, Oreste PP, Pelizza S, Poma A. Study of the influence of sub-horizontal fiber-glass pipes on the stability of a tunnel face. *Proceedings of Conference on North American Tunneling*'96, Washington. Balkema: Rotterdam, 1996.
7. Salençon J. Calcul à la rupture et analyse limite. *Presses de l'Ecole Nationale des Ponts et Chaussées*, Paris, 1983.
8. Davis EH, Gunn MJ, Mair RJ, Seneviratne HN. The stability of shallow tunnels and underground openings in cohesive material. *Geotechnique* 1980; **30**(4):397–416.
9. Leca E, Dormieux L. Upper and lower bound solutions for the face stability of shallow circular tunnels in frictional materials. *Geotechnique* 1990; **40**(4):581–606.
10. Leca E, Panet M. Application du calcul à la rupture à la stabilité du front de taille d'un tunnel. *Revue Française de Géotechnique* 1988; **43**:5–19.
11. Dias D, Kastner R, Dubois P. Tunnel face reinforcement by bolting: strain approach using 3D analysis, ITC Ltd, *Proceedings of International Conference on Tunnelling under Difficult Conditions*, Basel, 27–29 October 1997.
12. De Buhan P. Approche fondamentale du calcul à la rupture des ouvrages en sols renforcés, *Thèse de doctorat d'état ès Sciences Physiques*, Université Paris VI, 1986.
13. De Buhan P, Mangiavacchi R, Nova R, Pellegrini G, Salençon J. Yield design of reinforced earth walls by a homogenization approach. *Geotechnique* 1989; **39**(2):189–201.
14. Greuell E. Etude du soutènement des tunnels par boulons passifs dans les sols et les roches tendres, par une méthode d'homogénéisation. *Doctorate Thesis*, Ecole Polytechnique, France, 1993; 199 pp.
15. Wong H, Larue E. Modeling of bolting support in tunnels taking account of non-simultaneous yielding of bolts and ground, The Geotechnics of Hard Soils—Soft Rocks, *Proceedings of IInd International Conference*, Napoli 12–14 October 1998; 1027–1038.
16. Egger P. Deformation at the face of the heading and determination of the cohesion of the rock mass. *Underground Space Technology* 1980; **4**:313–318.
17. Panet M. Le calcul des tunnels par la méthode convergence-confinement, *Presses de l'Ecole Nationale des Ponts et Chaussées*, Paris, 1995.
18. Boutin C. Method of homogenization applied to civil engineering. *Thèse d'habilitation*, Ecole Nationale des Travaux Publics de l'Etat, Lyon, France, 1993 (in French).
19. Wong H, Jassionnesse C. Stabilité du front d'un tunnel renforcé par du boulonnage en fibre de verre, modèle analytique. *Proceedings of Symposium on GEO*, *Aussois*, France, 1996.
20. Wong H, Subrin D, Dubois P. Mouvements en avant due front de taille d'un tunnel renforcé par boulonnage: influence due comportement du sol. *Proceedings of Symposium on GEO*, Aussois, France, 24–28 November 1997.
21. Wong, H, Subrin D, Jassionnesse C. Comportement du front d'un tunnel renforcé par du boulonnage en fibre de verre, modèle analytique, *Géomatériaux-Environnement-Ouvrages*, vol. 2 Ouvrages, *Géomatériaux et Interactions*. Hermès: France, 1998; 133–147.
22. Jassionnesse C, Dubois P, Saïtta A. Tunnel face reinforcement by bolting, soil bolts homogenization strain approach. *Proceedings of Symposium on Geotechnical Aspects of Underground Constructions in Soft Ground*, London. Balkema: Rotterdam, 15–17 April 1996; 373–378.
23. Jassionnesse C. Contrôle de la déformation du massif renforcé par boulonnage au front de taille d'un tunnel, Etude de cas d'un cas réel en site urbain: exploitation des mesures et modélisation par une méthode d'homogénéisation. *Doctorate Thesis*, Institut National des Sciences Appliquées, Lyon, France, 1998; 233 pp.
24. Wong H. Thermoplastic and thermo-viscoplastic behaviours of underground cavities. *Proceedings of 8th International Congress of Society of Rock Mechanics*, Tokyo, 1995; 479–483.
25. Berest P. Problèmes de mécanique associés au stockage souterrain. *Doctorate Thesis*, Ecole Nationale Supérieure des Mines de Paris, 1989; 361 p.
26. Coatzee MJ, Hart RD, Varona PM, Cundall A. *FLAC Basics*, Itasca, Minneapolis, 1993.
27. Itasca Consulting Group, FLAC in 3D. *User Manual*, Minneapolis, 1994.
28. Dias D, Kastner R, Dubois P. Effects of pre-lining on the tunnel design. *Proceedings of International Conference on Underground Structures in Modern Infrastructure*, Stockholm. Balkema: Rotterdam, 7–9 June 1998.

29. Dias D, Subrin D, Wong H, Dubois P, Kastner R. Behaviour of a tunnel face reinforced by bolts: comparison between analytical-numerical models. The Geotechnics of Hard Soils—Soft Rocks, *Proceedings of IInd Conference*, Napoli 12–14 October 1998; 961–972.
30. Broms BB, Bennermark H. Stability of clay at vertical openings. ASCE, *Journal of Soil Mechanics Foundations Division* 1967; **SM1 93**:71–94.
31. Wong H, Trompille V, Subrin D, Guilloux A. Tunnel face reinforced by longitudinal bolts: analytical model and in situ data. *Proceedings of International Symposium on Geotechnical Aspects of Underground Construction in Soft Ground*. Tokyo, 1999; 435–440.
32. Wong H, Doanh T. EXTRUSION® Computer program and accompanying user manual. Ecole Nationale des Travaux Publics de l'Etat, Lyon, France, 1998.
33. Egger P, Subrin D, Wong H. Behavior of a tunnel head reinforced by bolting: experimental study and theoretical modeling. *Proceedings of 9th International Congress of Society of Rock Mechanics*, Paris, 1999; vol 1. 169–173.

